JACS
JOURNAL OF THE AMERICAN CHEMICAL SOCIETY
Communication
Cite This: J. Am. Chem. Soc. 2019, 141, 94−97
pubs.acs.org/JACS

TiO_2 Nanoparticles Catalyze Oxidation of Huntingtin Exon 1-Derived Peptides Impeding Aggregation: A Quantitative NMR Study of Binding and Kinetics

Alberto Ceccon, Vitali Tugarinov,* and G. Marius Clore*

Laboratory of Chemical Physics, National Institute of Diabetes and Digestive and Kidney Diseases, National Institutes of Health, Bethesda, Maryland 20892-0520, United States

Supporting Information

ABSTRACT: Polyglutamine expansion within the N-terminal region of the huntingtin protein results in the formation of intracellular aggregates responsible for Huntington's disease, a fatal neurodegenerative condition. The interaction between TiO_2 nanoparticles and huntingtin peptides comprising the N-terminal amphiphilic domain without (htt^{NT}) or with ($htt^{NT}Q_{10}$) a ten-residue C-terminal polyglutamine tract, is investigated by NMR spectroscopy. TiO_2 nanoparticles decrease aggregation of $htt^{NT}Q_{10}$ by catalyzing the oxidation of Met^7 to a sulfoxide, resulting in an aggregation-incompetent peptide. The oxidation agent is hydrogen peroxide generated on the surface of the TiO_2 nanoparticles either by UV irradiation or at low steady-state levels in the dark. The binding kinetics of nonaggregating htt^{NT} to TiO_2 nanoparticles is characterized by quantitative analysis of ^{15}N dark state exchange saturation transfer and lifetime line broadening NMR data. Binding involves a sparsely populated intermediate that experiences hindered rotational diffusion relative to the free state. Catalysis of methionine oxidation within the N-terminal domain of the huntingtin protein may potentially provide a strategy for delaying the onset of Huntington's disease.

Polyglutamine expansion within the N-terminal region of the huntingtin protein (corresponding to exon-1) favors aggregation and is responsible for Huntington's disease, a fatal neurodegenerative condition.[1] The polyglutamine domain lies downstream of the 16-residue N-terminal amphiphilic domain (htt^{NT}). Peptides comprising htt^{NT} with as few as 10 glutamines ($htt^{NT}Q_{10}$) aggregate rapidly in solution and form polymorphic fibrils.[2] We recently observed that oxidation of the Met^7 side-chain to a sulfoxide (Met^7) prevents aggregation of $htt^{NT}Q_{10}$.[3] In general, adsorption of fibril forming proteins and peptides on the surface of nanoparticles enhances aggregation and fibril formation by increasing the local peptide concentration and hence the probability of forming a critical initiation nucleus.[4,5] Titanium oxide nanoparticles (TiO_2 NPs) are unique as they possess photocatalytic properties that generate reactive oxygen species upon UV irradiation.[6,7] Here we study the interaction of htt^{NT} and $htt^{NT}Q_{10}$ with TiO_2 NPs by NMR, and show that TiO_2 NPs specifically catalyze the oxidation of Met^7, thereby preventing fibril formation by reducing the concentration of the aggregation-competent, native reduced form of $htt^{NT}Q_{10}$.

Spontaneous aggregation of $htt^{NT}Q_{10}$ occurs over time as monitored both by an increase in Thioflavin T (ThT) fluorescence emission (Figure 1A), attributed to the formation of β-rich amyloid-like structures, and by a decrease in the intensity of the amide proton envelope of the NMR signal (Figure 1B; see SI). Reduced and oxidized monomeric $htt^{NT}Q_{10}$ are NMR visible, while aggregates of reduced $htt^{NT}Q_{10}$ are broadened beyond detection, resulting in a decrease in the observable amide proton envelope intensity. Addition of photoexcited TiO_2 NPs (see SI and Figure S1) dramatically reduces the extent of aggregation. At 10 °C, only 8% of a 300 μM ^{15}N-$htt^{NT}Q_{10}$ sample remains NMR visible after 100 h; in the presence of photoexcited TiO_2 NPs, however, aggregation plateaus out with 33% of the sample remaining NMR visible (Figure 1B). The apparent aggregation $t_{1/2}$ (~23−25 h), however, is not affected by the TiO_2 NPs (Figure 1B). The reduction in the fraction of aggregating

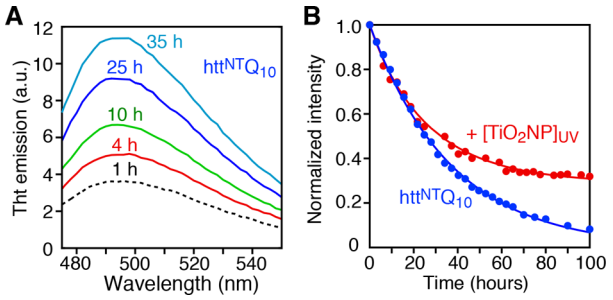

Figure 1. Effect of TiO_2 NPs on aggregation of $htt^{NT}Q_{10}$ monitored by NMR at 10 °C. Time course of (A) ThT emission of 25 μM $htt^{NT}Q_{10}$ in the absence of TiO_2 NPs, and (B) of the intensity of the amide proton envelope of 300 μM ^{15}N-labeled $htt^{NT}Q_{10}$ in the absence (blue circles) and presence (red circles) of 5 g·L^{-1} TiO_2 NPs photoexcited by exposure to UV light prior to addition to the peptide solution. The solid lines represent best fits where the disappearance of reduced, NMR visible $htt^{NT}Q_{10}$ (k_{agg} ~ 0.03 h^{-1}) due to aggregation competes with oxidation to aggregation-incompetent Met^7O-$htt^{NT}Q_{10}$ (see Scheme 1). The normalized intensities are corrected for sample to sample variations in the amounts of Met^7O-$htt^{NT}Q_{10}$ present at t = 0 (see SI).

Received: October 23, 2018
Published: December 12, 2018

DOI: 10.1021/jacs.8b11441
J. Am. Chem. Soc. 2019, 141, 94−97

species can be attributed to TiO_2 NP catalyzed oxidation of the side chain of Met[7] to a sulfoxide. Several reactive oxygen species are formed on the surface of TiO_2 NPs upon UV irradiation (Figure S2),[6,7] but only H_2O_2 is stable with significant amounts generated both upon UV irradiation and in the dark (Figures 2A and S3).

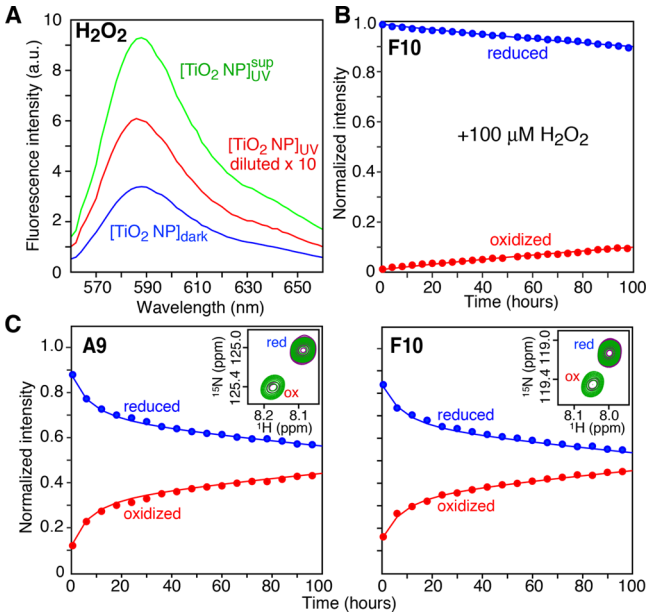

Figure 2. TiO_2-catalyzed oxidation of htt^{NT}. (A) Amplex Red assay for H_2O_2 generated by 5 g·L^{-1} TiO_2 NPs in the dark (blue, ~4 μM H_2O_2) and upon UV exposure for 3 h (red, NP suspension, ~76 μM H_2O_2; green, supernatant after removal of NPs, ~11 μM H_2O_2). (B) Time course of Met[7] oxidation of 300 μM ^{15}N-labeled htt^{NT} following addition of (B) 100 μM H_2O_2 and (C) UV-irradiated TiO_2 NPs (5 g·L^{-1}, 3 h UV exposure)monitored by the reduction and corresponding increase in intensities of Ala[9] and Phe[10] cross-peaks arising from reduced (blue) and Met[7]O oxidized (red) htt^{NT}, respectively, in a series of ^{1}H−^{15}N HSQC spectra. The insets in (C) show the cross-peaks corresponding to the reduced (upfield) and oxidized (downfield) states at t = 0 (purple) and 80 (green) hours. The experimental data in panels B and C are shown as circles and the best-fit curves obtained by nonlinear optimization and integration of the differential equations (eq S1) describing the oxidation process in Scheme 1 are represented by solid lines. The different ratios of oxidized to reduced htt^{NT} at time zero in panels (B) and (C) reflect sample to sample variations. Data were collected at 10 °C and a spectrometer frequency of 600 MHz.

The oxidation kinetics of $htt^{NT}Q_n$ huntingtin peptides (where n = number of glutamines in the polyglutamine tract) in the presence of TiO_2 NPs can be described by three parallel reactions (Scheme 1): two second-order processes involving oxidation of $htt^{NT}Q_n$ (P_{red}) to Met[7]O-$htt^{NT}Q_n$ (P_{oxi}) by H_2O_2, generated upon UV irradiation, either dissolved in solution (k_1) or on the surface of the TiO_2 NPs (k_2), and a pseudo-first-order process ($k_3^{dark} = k_2[H_2O_2]_{dark}$) occurring in the dark that involves a low steady-state (i.e., continuously generated) level of H_2O_2 on the surface of the TiO_2 NPs.[8] These reactions occur concomitantly with aggregation of P_{red} which, for simplicity, is described as a unimolecular process with a rate constant k_{agg}. Our treatment of the kinetics of all oxidative processes assumes that oxidation proceeds on a time-scale much slower than that of binding to TiO_2 NPs, as is amply confirmed experimentally (see below).

Scheme 1. Parallel Reactions Describing Aggregation and TiO_2 NP-Catalyzed Oxidation of $htt^{NT}Q_n$ Peptides

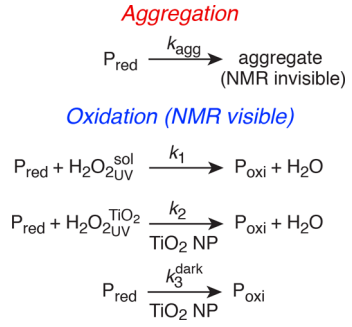

To study the kinetics of TiO_2 catalyzed oxidation of huntingtin peptides in the absence of aggregation (k_{agg} = 0 in Scheme 1), we made use of a peptide comprising only the N-terminal amphiphilic domain, htt^{NT}, which remains stable in the presence of TiO_2 NPs for many days (Figure S4). Oxidation of htt^{NT} by H_2O_2 free in solution makes an insignificant contribution to the kinetics of htt^{NT} oxidation in the presence of 5 g·L^{-1} TiO_2 NPs as the concentration of dissolved H_2O_2 generated upon UV irradiation (~11 μM, Figure 2A) is 10-fold lower than that used in the experiment with added H_2O_2 shown in Figure 2B. The time course of oxidation in the presence of UV irradiated TiO_2 is biphasic (Figure 2C). The first phase arises from second-order (k_2 ~ 500 M^{-1} h^{-1}) oxidation of Met[7] by the substantial amount of H_2O_2 located on the surface of the TiO_2 NPs generated by UV irradiation. Oxidation on the TiO_2 NP surface is accelerated ~45-fold relative to that free in solution. Once H_2O_2 generated by UV irradiation is consumed, a slower apparent first order oxidation process ($k_3^{dark} = k_2[H_2O_2]_{dark}$ ~ 0.002 h^{-1}) occurs owing to the steady-state level of H_2O_2 present on the TiO_2 NP surface in the dark. With these values of k_2 and k_3^{dark}, Scheme 1 quantitatively accounts for the disappearance of NMR visible $htt^{NT}Q_{10}$ in the presence of photoactivated TiO_2 NPs with k_{agg} ~ 0.03 h^{-1} which remains unchanged in the absence of TiO_2 NPs (Figure 1B).

The efficiency of heterogeneous catalysis is dependent upon the strength of interaction between the adsorbate (htt^{NT}) and the surface of the catalyst.[9] We therefore characterized the kinetic and mechanistic details of ^{15}N-labeled htt^{NT} adsorption on the surface of TiO_2 NPs using ^{15}N dark state exchange saturation transfer (DEST) and lifetime line broadening (ΔR_2) which enable one to quantitatively analyze exchange processes between an NMR visible species and very high molecular weight, NMR invisible "dark" states.[10−13] Although binding of $htt^{NT}Q_{10}$ to TiO_2 NPs cannot be studied quantitatively owing to $htt^{NT}Q_{10}$ aggregation during the time course of the DEST experiment (several days), ΔR_2 measurements are sufficiently fast (a few hours) to demonstrate significant ^{15}N lifetime line broadening (~10 s^{-1}), and hence binding, of $htt^{NT}Q_{10}$ in the presence of TiO_2 NPs (Figure S5).

Examples of ^{15}N-DEST profiles and a plot of ^{15}N-ΔR_2 as a function of residue for reduced htt^{NT} in the presence of TiO_2 NPs in the dark are shown in Figure 3A,B, respectively. These conditions correspond to a quasi-equilibrium state where Met[7] oxidation by the small amount of steady-state H_2O_2 generated on the TiO_2 NP surface in the dark proceeds very slowly ($t_{1/2}$ ~ 350 h). The shapes of the ^{15}N-DEST profiles are unusual and characterized by a narrow component superimposed on a

DOI: 10.1021/jacs.8b11441
J. Am. Chem. Soc. 2019, 141, 94−97

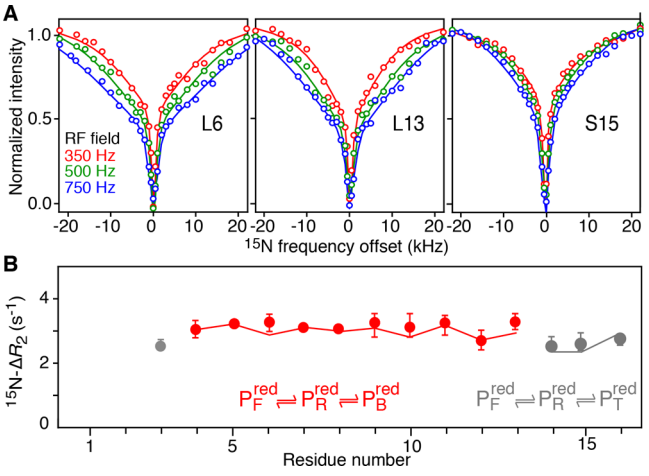

Figure 3. Kinetics of htt^{NT} binding to TiO_2 NPs characterized by relaxation-based NMR. (A) Examples of ^{15}N-DEST profiles and (B) ^{15}N-ΔR_2 as a function of residue observed for 300 μM ^{15}N-labeled htt^{NT} in the presence of 5 g·L^{-1} TiO_2 NPs in the dark. Circles represent experimental data, and solid lines are best fits to a three-state exchange model. Residues requiring a separate treatment are shown in gray. Data were recorded at 600 MHz and 10 °C.

broad one (Figure 3A) indicative of a three-state exchanging system in which the slow exchange process due to htt^{NT} binding to the TiO_2 NP surface is accompanied by a second exchange process occurring on a much faster time scale. The ^{15}N-DEST and ΔR_2 data were fit simultaneously to the three-state exchange model shown in red in Figure 3B via propagation of a set of Bloch-McConnell[14] equations.

Exchange between free (P_F^{red}) and TiO_2 NP-bound (P_B^{red}) htt^{NT} monomer proceeds via an intermediate (P_R^{red}) whose rotational diffusion is only partially restricted, presumably due to initial binding to the hydration layer surrounding the TiO_2 NP; the final bound state experiences the same rotational diffusion as the TiO_2 NP itself (Figure 4). This binding mechanism is similar to that observed for the adsorption of cholic acid to ceria NPs.[15]

The population (p_B^{red} = 1.7 ± 0.1%) of TiO_2 NP-bound reduced htt^{NT}, the rate constant k_{BR} (97 ± 5 s^{-1}) for the transition from fully bound to partially restricted states, and the transverse relaxation rates in the bound state (<^{15}N-R_2^{bound}> = 31 000 ± 300 s^{-1}) are well-defined from the fits. The population of the intermediate state (p_R^{red}), however, cannot

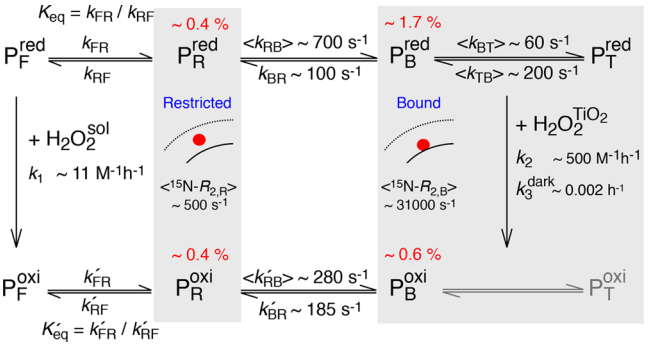

Figure 4. Overall kinetic scheme for the binding htt^{NT} to TiO_2 NPs coupled with oxidation of htt^{NT} to the Met^7 sulfoxide form either in solution or on the NP surface. States in contact with TiO_2 NPs are shaded.

be determined with certainty without assumptions regarding the magnitude of its transverse spin relaxation rate, ^{15}N-$R_2^{restricted}$. This is due to fast interconversion between P_F^{red} and P_R^{red} on the relaxation time-scale ($k_{FR} + k_{RF} \gg R_2^{restricted}$), so that extraction of k_{FR}, k_{RF} and ^{15}N-$R_2^{restricted}$ is not possible without assumptions regarding these parameters. Thus, only ranges of ^{15}N-$R_2^{restricted}$ and p_R^{red} could be established (see SI): for <^{15}N-$R_2^{restricted}$> = 200 to 750 s^{-1}, p_R^{red} varies from 0.5 to 0.2%. Although populated at less than 1%, the inclusion of P_R^{red} into the analysis is essential to reproduce the experimental ^{15}N-DEST profiles.

The ^{15}N-DEST/ΔR_2 data for Leu^3 and the C-terminal three residues of htt^{NT} required a separate treatment and were fitted to the three-state model shown in gray in Figure 3B. Although formally the same overall three-state exchange model is used for these residues ($P_F^{red} \leftrightarrow P_R^{red} \leftrightarrow P_T^{red}$), the exchange process subsumes initial binding to the NP surface followed by reversible detachment from the surface (state P_T^{red}, where "T" denotes "tethered").[13] The rate constants k_{BT} and k_{TB} were calculated *a-posteriori* (see SI and Figure 4) and fall in the ranges 40 to 75 s^{-1} and 160 to 240 s^{-1}, respectively, depending on the assumed population of state P_R^{red}. It follows that reversible detachment of these 4 residues from the NP surface occurs ~3-fold slower than the binding event proper ($P_R^{red} \leftrightarrow P_B^{red}$). While the central residues of htt^{NT} are likely to form an ordered helical structure when bound to TiO_2 NPs, as observed for htt^{NT}Q$_n$ peptides bound to lipid micelles,[3] the parts of the peptide that remain unstructured in the bound state retain the flexibility of the free peptide and can transiently detach from the NP surface (i.e., they are "tethered"). The same phenomenon was also observed in the interaction of htt^{NT}Q$_n$ with small unilamellar lipid vesicles.[13]

The binding of Met^{7}O-htt^{NT} to TiO_2 NPs was also characterized by analysis of ^{15}N-DEST and ΔR_2 data (Figure S6). The population of the bound state P_B^{oxi} is ~0.6%, ~3-fold lower than that of the reduced form, indicating that oxidation of Met^7 reduces the binding affinity to TiO_2 NPs, in agreement with previous studies on the interaction of htt^{NT}Q$_7$ with lipid micelles.[3]

In conclusion, the current work provides a mechanistic basis for understanding the interaction of huntingtin peptides with TiO_2 NPs coupled with surface-catalyzed oxidation, and suggests that targeted catalysis of Met^7 oxidation within the htt^{NT} domain of the huntingtin protein may provide a strategy for delaying the onset of Huntington's disease.

■ ASSOCIATED CONTENT

Supporting Information

The Supporting Information is available free of charge on the ACS Publications website at DOI: 10.1021/jacs.8b11441.

Experimental details, fitting procedures and three additional figures (PDF)

■ AUTHOR INFORMATION

Corresponding Authors

*mariusc@mail.nih.gov

*vitali.tugarinov@nih.gov

ORCID

G. Marius Clore: 0000-0003-3809-1027

Notes

The authors declare no competing financial interest.

DOI: 10.1021/jacs.8b11441
J. Am. Chem. Soc. 2019, 141, 94−97

■ ACKNOWLEDGMENTS

We thank James Baber, Dan Garrett and Jinfa Ying for NMR and computational support. This work was supported by the Intramural Research Program of the National Institute of Diabetes and Digestive and Kidney Diseases, NIH (to G.M.C.).

■ REFERENCES

(1) Andresen, J. M.; Gayan, J.; Djousse, L.; Roberts, S.; Brocklebank, D.; Cherny, S. S.; Cardon, L. R.; Gusella, J. F.; MacDonald, M. E.; Myers, R. H.; Housman, D. E.; Wexler, N. S. The Relationship between Cag Repeat Length and Age of Onset Differs for Huntington's Disease Patients with Juvenile Onset or Adult Onset. *Ann. Hum. Genet.* **2007**, *71*, 295−301.

(2) Jayaraman, M.; Kodali, R.; Sahoo, B.; Thakur, A. K.; Mayasundari, A.; Mishra, R.; Peterson, C. B.; Wetzel, R. Slow Amyloid Nucleation Via α Helix-Rich Oligomeric Intermediates in Short Polyglutamine-Containing Huntingtin Fragments. *J. Mol. Biol.* **2012**, *415*, 881−99.

(3) Ceccon, A.; Schmidt, T.; Tugarinov, V.; Kotler, S. A.; Schwieters, C. D.; Clore, G. M. Interaction of Huntingtin Exon-1 Peptides with Lipid-Based Micellar Nanoparticles Probed by Solution NMR and Q-Band Pulsed EPR. *J. Am. Chem. Soc.* **2018**, *140*, 6199−6202.

(4) Linse, S.; Cabaleiro-Lago, C.; Xue, W. F.; Lynch, I.; Lindman, S.; Thulin, E.; Radford, S. E.; Dawson, K. A. Nucleation of Protein Fibrillation by Nanoparticles. *Proc. Natl. Acad. Sci. U. S. A.* **2007**, *104*, 8691−6.

(5) Wu, W. H.; Sun, X.; Yu, Y. P.; Hu, J.; Zhao, L.; Liu, Q.; Zhao, Y. F.; Li, Y. M. TiO_2 Nanoparticles Promote β-Amyloid Fibrillation in Vitro. *Biochem. Biophys. Res. Commun.* **2008**, *373*, 315−8.

(6) Schneider, J.; Matsuoka, M.; Takeuchi, M.; Zhang, J.; Horiuchi, Y.; Anpo, M.; Bahnemann, D. W. Understanding TiO_2 Photocatalysis: Mechanisms and Materials. *Chem. Rev.* **2014**, *114*, 9919−86.

(7) Nosaka, Y.; Nosaka, A. Y. Generation and Detection of Reactive Oxygen Species in Photocatalysis. *Chem. Rev.* **2017**, *117*, 11302−11336.

(8) Jayaram, D. T.; Runa, S.; Kemp, M. L.; Payne, C. K. Nanoparticle-Induced Oxidation of Corona Proteins Initiates an Oxidative Stress Response in Cells. *Nanoscale* **2017**, *9*, 7595−7601.

(9) Schauermann, S.; Nilius, N.; Shaikhutdinov, S.; Freund, H. J. Nanoparticles for Heterogeneous Catalysis: New Mechanistic Insights. *Acc. Chem. Res.* **2013**, *46*, 1673−1681.

(10) Fawzi, N. L.; Ying, J.; Torchia, D. A.; Clore, G. M. Kinetics of Amyloid Beta Monomer-to-Oligomer Exchange by NMR Relaxation. *J. Am. Chem. Soc.* **2010**, *132*, 9948−9951.

(11) Fawzi, N. L.; Ying, J.; Ghirlando, R.; Torchia, D. A.; Clore, G. M. Atomic-Resolution Dynamics on the Surface of Amyloid β Protofibrils Probed by Solution NMR. *Nature* **2011**, *480*, 268−272.

(12) Ceccon, A.; Tugarinov, V.; Bax, A.; Clore, G. M. Global Dynamics and Exchange Kinetics of a Protein on the Surface of Nanoparticles Revealed by Relaxation-Based Solution NMR Spectroscopy. *J. Am. Chem. Soc.* **2016**, *138*, 5789−5792.

(13) Ceccon, A.; Clore, G. M.; Tugarinov, V. Decorrelating Kinetic and Relaxation Parameters in Exchange Saturation Transfer NMR: A Case Study of N-Terminal Huntingtin Peptides Binding to Unilamellar Lipid Vesicles. *J. Phys. Chem. B* **2018**, DOI: 10.1021/acs.jpcb.8b07112.

(14) McConnell, H. M. Reaction Rates by Nuclear Magnetic Resonance. *J. Chem. Phys.* **1958**, *28*, 430−431.

(15) Egner, T. K.; Naik, P.; Nelson, N. C.; Slowing, II; Venditti, V. Mechanistic Insight into Nanoparticle Surface Adsorption by Solution NMR Spectroscopy in an Aqueous Gel. *Angew. Chem., Int. Ed.* **2017**, *56*, 9802−9806.

DOI: 10.1021/jacs.8b11441
J. Am. Chem. Soc. 2019, 141, 94−97